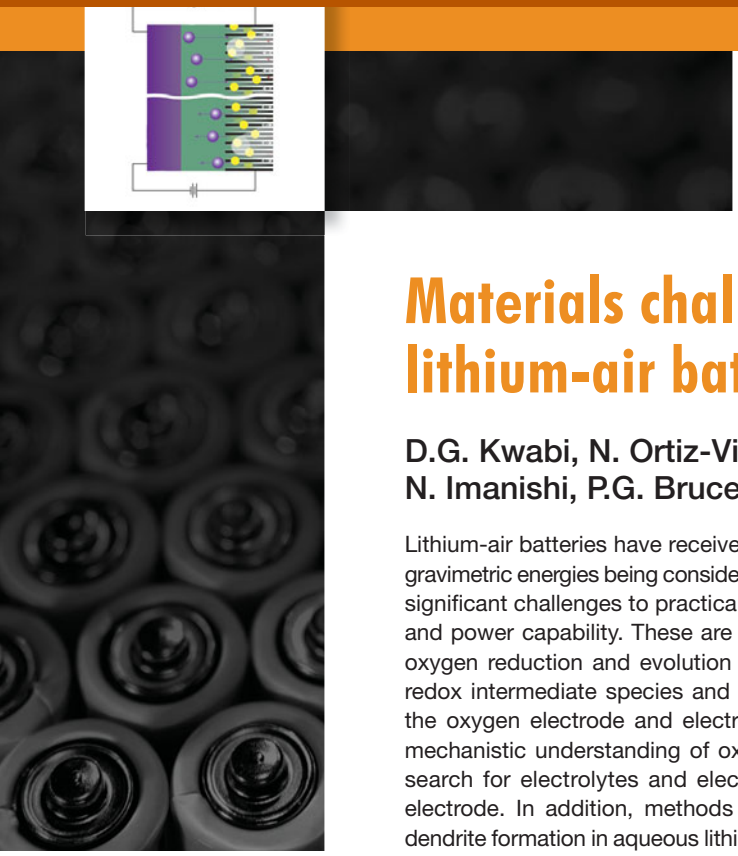

# Materials challenges in rechargeable lithium-air batteries

D.G. Kwabi, N. Ortiz-Vitoriano, S.A. Freunberger, Y. Chen, N. Imanishi, P.G. Bruce, and Y. Shao-Horn

Lithium-air batteries have received extraordinary attention recently owing to their theoretical gravimetric energies being considerably higher than those of Li-ion batteries. There are, however, significant challenges to practical implementation, including low energy efficiency, cycle life, and power capability. These are due primarily to the lack of fundamental understanding of oxygen reduction and evolution reaction kinetics and parasitic reactions between oxygen redox intermediate species and nominally inactive battery components such as carbon in the oxygen electrode and electrolytes. In this article, we discuss recent advances in the mechanistic understanding of oxygen redox reactions in nonaqueous electrolytes and the search for electrolytes and electrode materials that are chemically stable in the oxygen electrode. In addition, methods to protect lithium metal against corrosion by water and dendrite formation in aqueous lithium-air batteries are discussed. Further materials innovations lie at the heart of research and development efforts that are needed to enable the development of lithium-oxygen batteries with enhanced round-trip efficiency and cycle life.

## Introduction

The need to store electricity is becoming increasingly critical to link energy supply to our energy demands as we shift from the use of fossil fuels to renewable energy sources such as solar and wind. Advances in the past two decades in electrochemical energy storage technologies such as Li-ion batteries have enabled the ubiquity of mobile electronic devices in our lives. The expansion of electrified transportation to driving ranges of ~300 miles per recharge, as offered by vehicles based on internal combustion engines, and the use of intermittent solar and wind energy for stationary power applications call for storage technologies with much greater gravimetric energies than Li-ion batteries. Energy storage schemes that involve the transfer of multiple electrons during discharge such as lithium-air[1] and zinc-air batteries,[2] as well as Li-S batteries (see the Nazar et al. article in this issue), can provide higher gravimetric energies than Li-ion batteries that are constrained largely to one-electron intercalation.[1–3] Although the basic principle behind the operation of metal-air batteries (or more accurately metal-$O_2$ since only the $O_2$ drawn from the air is used; other reactive constituents [e.g., $CO_2$] need to be excluded to a sufficient level) is well known, there are immense challenges to overcome in order to make these technologies practical and to do so with a battery that delivers the promised step-change in energy storage. In this article, we discuss some key materials challenges and highlight recent advances in Li-$O_2$ battery research.

The operation of Li-$O_2$ batteries is based on the conversion of stored chemical energy in lithium (fuel) and oxygen into electrical energy via the formation of reaction products containing lithium ions and reduced oxygen species.[4–6] This scheme incorporates operational elements of a fuel cell (e.g., reduction of gaseous $O_2$ from the environment during discharge) with that of a battery (storage of electrons and $Li^+$ in the oxygen electrode), and therefore represents a departure from conventional constraints of Li-ion positive electrode development. Li-$O_2$ batteries differ from Li-ion batteries in that rather than intercalating lithium into a host lattice containing transition metal ions (see the Introductory article in this issue), oxygen is reduced to solid $Li_2O_2$, filling the pore

D.G. Kwabi, Massachusetts Institute of Technology, USA; dkwabi@mit.edu
N. Ortiz-Vitoriano, Massachusetts Institute of Technology, USA; nagore@mit.edu
S.A. Freunberger, Graz University of Technology, Austria; freunberger@tugraz.at
Y. Chen, University of St. Andrews, UK; yc21@st-andrews.ac.uk
N. Imanishi, Mie University, Japan; imanishi@chem.mie-u.ac.jp
P.G. Bruce, University of St. Andrews, UK; pgb1@st-andrews.ac.uk
Y. Shao-Horn, Massachusetts Institute of Technology, USA; shaohorn@mit.edu
DOI: 10.1557/mrs.2014.87

spaces of the oxygen electrode in nonaqueous electrolytes and soluble LiOH in aqueous electrolytes.

The replacement of intercalation cathodes containing heavy transition metal ions that typically undergo 1 electron redox reaction with $O_2$ from air that undergoes 2 electron redox reactions offers the possibility of higher gravimetric energy. As the $O_2$ is available from the air, the cost is potentially lower than Li-ion batteries. Using nonaqueous electrolytes and lithium as the negative electrode, Li-$O_2$ batteries have an upper gravimetric energy limit of ~3500 Wh/$kg_{Li_2O_2}$ [3,7–10] (or ~3500 Wh/$kg_{cell}$ considering the cell weight with lithium and oxygen only), where oxygen is reduced to form $Li_2O_2$ ($2Li + O_2 \leftrightarrow Li_2O_2$; 2.96 V versus $Li/Li^+$). In contrast, Li-$O_2$ batteries that use aqueous electrolytes and lithium as the negative electrode, where LiOH is formed ($2Li + 1/2O_2 + H_2O \leftrightarrow 2LiOH$; 3.2 V versus $Li/Li^+$[11]), have lower gravimetric energies, with upper limits of ~700–1000 Wh/$kg_{cell}$ (considering the cell weight with lithium, oxygen, and seven to twelve-fold excess water).[3,11,12] If gravimetric energy densities are calculated based on lithium metal alone, then much higher numbers are obtained,[5,13] but one cannot neglect the mass of $O_2$ and water.

Despite the fact that the estimated upper limits of gravimetric energy for Li-$O_2$ batteries vary depending on different assumptions used in the oxygen electrode[1] reported previously, they are at least ~2–3 times higher than those of state-of-the-art Li-ion batteries.[1–3] It is important to recall that in energy storage there is no equivalent of Moore's Law that describes a doubling of performance every 18 months in microelectronic devices (e.g., floating point operations per second or data storage per chip footprint area). Additionally, these large gravimetric energy gains offered by Li-$O_2$ chemistry can be fully realized only if lithium instead of conventional Li-ion negative electrode materials such as carbon is used due to the much greater gravimetric capacity of lithium (3861 mAh/$g_{Li}$, $Li^+ + e^- \rightarrow Li$) compared to carbon (372 mAh/$g_C$, $Li^+ + C_6 + e^- \rightarrow LiC_6$).[14] In this article, we will consider individually the challenges and opportunities for nonaqueous and aqueous Li-$O_2$ batteries, with a particular focus on the current understanding of the reaction mechanisms and the materials used, which are issues that must be addressed in transforming these batteries from theory to practice.

## Challenges and opportunities: Nonaqueous Li-$O_2$ batteries

Notable progress has been made in the development of rechargeable nonaqueous Li-$O_2$ batteries in the past five years. Work to date has enabled prototypical lab-scale demonstration of significant gravimetric energy density enhancements of Li-$O_2$ positive electrodes (**Figure 1**a) compared to state-of-the-art lithium-ion electrodes such as $LiCoO_2$,[15] $LiFePO_4$,[16] and $LiNi_{0.5}Mn_{0.5}O_2$.[17] Reported gravimetric energy densities of cells based on oxygen electrodes[4,9,10] upon first discharge are ~3 times higher than those based on Li-ion positive electrodes (~600 Wh/$kg_{cell}$),[17,18] as shown in Figure 1b. It is important to note that the gravimetric energies for Li-$O_2$ systems only include the weight of carbon, $Li_2O_2$, and a metallic lithium anode, which are necessary to fairly compare the potential of the oxygen electrode relative to conventional Li-ion positive electrodes. Packaged Li-$O_2$ cell prototypes have not been widely developed, and the true gravimetric energy advantage of practical devices is not known. It is too early in the exploration of Li-$O_2$ battery technology to make accurate predictions of practical energy storage. Since the nature of the electrodes or electrolytes that might be used in a practical system are unknown, their tolerance to constituents in the air other than $O_2$ (e.g., $CO_2$) and the nature of any $O_2$ filtration approaches that might have to be taken to operate in air are also unknown. Additionally, if Li metal is used as the anode, the excess of Li that might be required in a new generation of protected Li anodes is as yet unknown. Such issues need to be investigated before hard-and-fast evidence-based estimates of practical performance can be made.

Unfortunately, rechargeable nonaqueous Li-$O_2$ batteries currently suffer from low round-trip efficiency (energy delivered on discharge divided by energy consumed on charge), cycle life, and power capability,[1,3–5,19] which limits their practical use. These performance challenges result, in part, from a lack of fundamental understanding of the mechanisms of oxygen reduction and evolution reactions in the oxygen electrode. Challenges also include the chemical instability of active and inactive components, including the dimensional stability

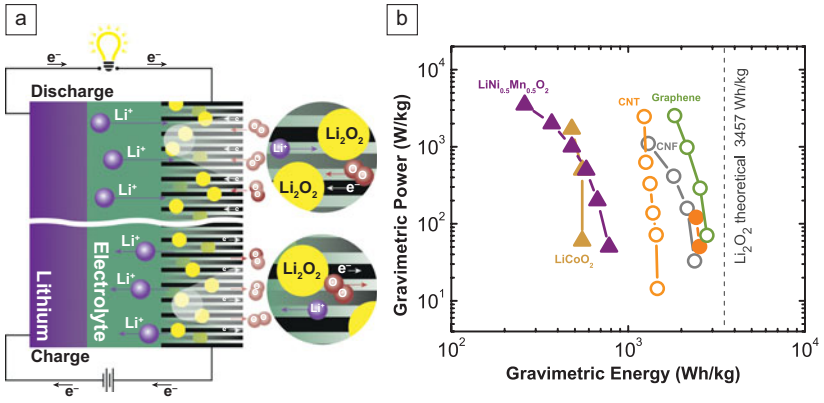


**Figure 1.** (a) Working principles of an Li-$O_2$ cell and (b) gravimetric Ragone plot (power versus energy) of reported discharged Li-$O_2$ cells containing various carbon cathodes: carbon nanotubes (CNTs),[8] carbon nanofibers (CNFs),[20] and freestanding hierarchically porous carbon ("graphene").[10] Cells based on conventional Li-ion positive electrodes, $LiCoO_2$[18] and $LiNi_{0.5}Mn_{0.5}O_2$,[17] coupled with Li anodes for direct comparison are shown. Note that for Li-$O_2$ cells, the total mass of the cathode was used (carbon + $Li_2O_2$). Open orange circles are for CNTs discharged to a limited capacity of 1,000 mAh/$g_C$, while closed orange circles are from CNT electrodes discharged to 5,000 mAh/$g_C$.[19] The theoretical gravimetric energy of $Li_2O_2$ is calculated assuming a discharge voltage of 2.96 V versus Li and 1168 mAh/g $Li_2O_2$.

of metallic lithium during repeated oxidation and plating, the chemical stability of conventional current collector materials for the oxygen electrode (such as carbon), and nonaqueous electrolytes in the oxygen electrode. In the first part of this article, we discuss recent research findings that highlight the current understanding of oxygen reduction and evolution reactions in nonaqueous electrolytes and the state of the search for chemically stable nonaqueous electrolytes and porous cathode substrates.

Using vertically aligned carbon nanotubes (CNTs) as the oxygen electrode has provided valuable insights into the mechanism of oxygen reduction and evolution reactions, specifically $Li_2O_2$ growth and oxidation mechanisms and the relationship between $Li_2O_2$ morphology/chemistry and the voltage penalty, or overpotential, associated with $Li_2O_2$ growth and oxidation. Toroidal structures of $Li_2O_2$ (**Figure 2**a), with sizes of hundreds of nanometers, form upon discharge at high discharge potentials (greater than 2.7 $V_{Li}$). The aspect ratio of the toroids are scaled with the toroidal diameter, while small $Li_2O_2$ particles (Figure 2b, <20 nm) are formed conformally on CNTs at discharge voltages lower than 2.7 $V_{Li}$.[10,20–22] Toroidal morphologies are characteristic of electrochemically formed $Li_2O_2$, and they have been observed in a broad range of non-carbonate electrolytes (ethers and dimethyl sulfoxide [DMSO]).[10,22,23] Mitchell et al.[23] have shown that these toroids are composed of thin plates of epitaxially oriented $Li_2O_2$, ~10 nm in thickness with the $(001)_{Li_2O_2}$ direction normal to the plate surface (Figure 2c–d). Recent surface-sensitive x-ray absorption near edge structure (XANES) findings suggest that although $Li_2O_2$ is invariably formed upon battery discharge, the electronic structure of the surfaces of the toroids have oxygen-rich $LiO_2$-like species (Figure 2f), while the conformally coated particles retain a more stoichiometric $Li_2O_2$-related configuration. These findings are in agreement with recent theoretical calculations that reported the thermodynamically stable $(001)_{Li_2O_2}$ surface of $Li_2O_2$, which is the dominant surface termination of toroidal $Li_2O_2$ particles, should possess $LiO_2$-like character.[24]

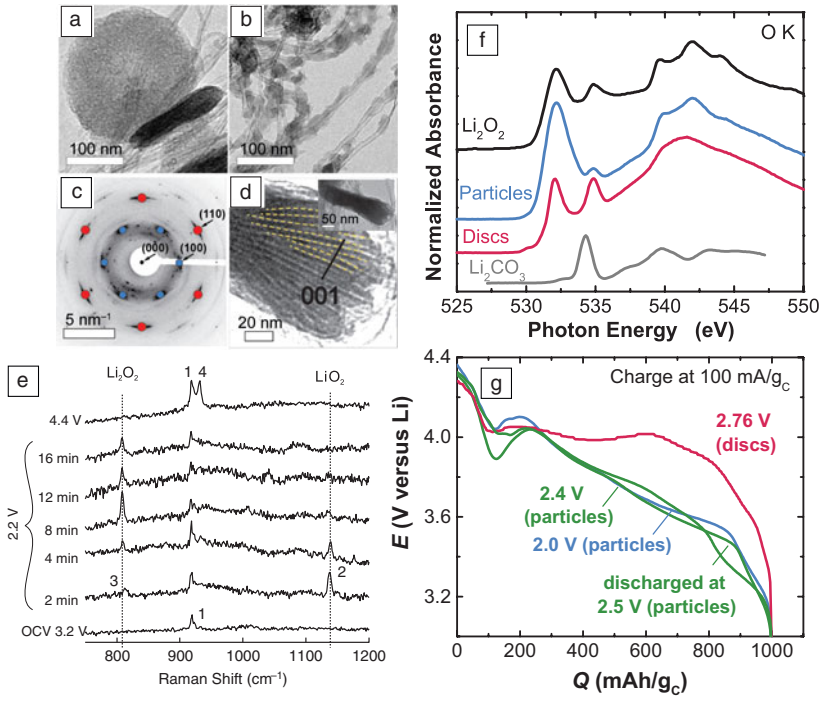


**Figure 2.** Transmission electron microscopy (TEM) images of carbon nanotube (CNT) electrodes discharged at (a) 10 mA/g to 4000 mAh $g_C^{-1}$ showing $Li_2O_2$ toroids, (b) 2.4 V to 5,000 mAh $g_C^{-1}$, (c) electron diffraction patterns of toroidal $Li_2O_2$, and (d) high-resolution TEM imaging of [001]-oriented $Li_2O_2$ plates, with lower magnification in inset. Reproduced with permission from References 19 and 23. © 2013 American Chemical Society. (e) *In situ* surface-enhanced Raman spectra during oxygen reduction reaction (ORR) and oxygen evolution reaction (OER) on an Au electrode in $O_2$-saturated electrolyte. The peaks are assigned as follows: (1) C–C stretch of $CH_3CN$ at 918 $cm^{-1}$, (2) O–O stretch of $LiO_2$ at 1137 $cm^{-1}$, (3) O–O stretch of $Li_2O_2$ at 808 $cm^{-1}$, and (4) Cl–O stretch of $ClO_4$ at 931 $cm^{-1}$. Adapted with permission from Reference 25. (f) Surface-sensitive x-ray absorption near-edge structure O–K edge data of toroids formed at 10 mA/g to 4,000 mAh $g_C^{-1}$ and particles formed at 2.4 V to 5,000 mAh $g_C^{-1}$ showing that particles closely resemble stoichiometric $Li_2O_2$, while toroids exhibit $LiO_2$-like features. (g) Constant-current charging of $Li_2O_2$ discharged at 2.0, 2.4, 2.5, and 2.76 V versus Li/$Li^+$ at 100 mA/$g_C$, showing the evolution of charge potential (*E*) with charge capacity (*Q*), with particle charging occurring at a lower average voltage penalty than toroid oxidation. Reprinted with permission from References 19 and 23. © 2013 American Chemical Society.

The differences in the morphology and surface chemistry of $Li_2O_2$ particles may be explained by the following oxygen reduction elementary reaction steps[25] in nonaqueous electrolytes:

$$O_2 + e^- \rightarrow O_2^-$$

$$Li^+ + O_2^- \rightarrow LiO_2$$

$$2LiO_2 \rightarrow Li_2O_2 + O_2$$

or

$$Li^+ + LiO_2 + e^- \rightarrow Li_2O_2$$

The appearance of $LiO_2$ as an intermediate (Figure 2e), followed by a disproportionation or a second electron transfer reaction to form $Li_2O_2$, is supported in work by Peng et al.[25] using *in situ* surface-enhanced Raman spectroscopy (SERS). At high discharge potentials (low overpotentials), the growth of toroidal $Li_2O_2$ particles may involve the formation of soluble reaction intermediate species such as $O_2^-$ and $LiO_2$ and the growth of $Li_2O_2$ by chemical disproportion of $LiO_2$.[26,27] These findings suggest that the increasing surface area associated with the increasing disc diameter during discharge promotes $Li_2O_2$ growth onto the disc surfaces, leading to the development of thick, toroidal particles. Lowering the discharge potential (increasing the overpotential) promotes

the kinetics of the second electron transfer step such that soluble reaction intermediates are reduced to form $Li_2O_2$ conformally coated on CNTs before they diffuse.

Differences in the morphology and surface chemistry of $Li_2O_2$ toroids and conformally coated particles on CNTs appear to influence $Li_2O_2$ oxidation kinetics.[19] Upon charging at low rates, the oxidation of conformally coated $Li_2O_2$ particles on CNTs exhibit a solid-solution-like voltage profile, while oxidation of $Li_2O_2$ toroids yields two-phase oxidation with a higher voltage penalty (Figure 2g). Although the physical origin of this observed difference is not fully understood, it is hypothesized[19] that the oxidation kinetics of $Li_2O_2$ are dependent on surface termination. Thus, the oxidation of $Li_2O_2$ particles coated on CNTs with multiple facets can occur at different voltages, giving rise to the sloping voltage in contrast to toroidal particles with predominantly $(001)_{Li_2O_2}$ surface terminations. This work highlights the need to understand how the surface chemistry and microstructure of discharged $Li_2O_2$ influence oxygen evolution reaction (OER) kinetics and opens up potential opportunities to explore nucleation and growth mechanisms of $Li_2O_2$ particles for high-energy and/or high-power Li-$O_2$ batteries.

More interestingly, electron rather than lithium-ion transport limits the electrochemical oxidation kinetics of $Li_2O_2$ when the oxidation current is not limited by charge transfer kinetics under large overpotentials. This was shown in recent *in situ* transmission electron microscopy (TEM) imaging experiments with solid-state microbatteries[28] consisting of Si nanowires (NWs) coated with Li-ion-conducting solid electrolyte contacting $Li_2O_2$ particles. In particular, as shown in **Figure 3**, the oxidation of toroidal $Li_2O_2$ particles at very high overpotentials is initiated preferentially at the CNT/$Li_2O_2$ interface, as evidenced by the development of a light-contrast stripe beginning along the CNT axes (highlighted by the dashed red lines) of the CNT bundle contacting the $Li_2O_2$ particle. The formation of the light-contrast stripe in TEM can be explained by the thinning of $Li_2O_2$ particles at the $Li_2O_2$/CNT interface associated with electrochemical oxidation of $Li_2O_2$ ($Li_2O_2 \rightarrow 2Li^+ + O_2 + 2e^-$) and the concurrent release of $O_2$, while lithium ions migrate through the solid electrolyte coating the Si NW, and electrons flow through CNTs to the Au substrate.

The preferential oxidation at the MWCNT (multiwalled CNT)/$Li_2O_2$ interface, but not at the interface between $Li_2O_2$/solid electrolyte/Si, suggests that electrochemical oxidation kinetics of $Li_2O_2$ is electron-transport-limited instead of lithium-ion-transport-limited at very high overpotentials. These findings suggest that electrodes with large specific surface area to maximize the $Li_2O_2$/electrode interfacial area and high electronic conductivity to provide facile electron transport to reaction sites are desirable for the design of high rate rechargeable Li-$O_2$ batteries.

## Stability of inactive components in the oxygen electrode

Understanding the stability of inactive electrode components in Li-$O_2$ batteries is an intensive area of research since their stability is a major factor determining rechargeability and cycle life.[29–35] Differential electrochemical mass spectrometry (DEMS) experiments on isotopically labeled $^{13}C$ cathodes have suggested that after discharge, a thin layer of $Li_2CO_3$ is present between $Li_2O_2$ and carbon.[29] This hypothesis is supported by XANES studies[8] on discharged CNTs in Li-$O_2$ batteries, which show that $Li_2CO_3$ is present at the interface between $Li_2O_2$ and the CNT walls on first discharge, and suggest that carbon is not chemically stable during the oxygen reduction reaction (ORR) and is potentially reactive against $Li_2O_2$ and ORR intermediates such as $O_2^-$ and $LiO_2$.

Recent *in situ* ambient pressure x-ray photoelectron spectroscopy (XPS) measurements further demonstrate the instability of carbon during ORR[30] at the interface between graphene and a solid-state lithium ion conductor (with no nonaqueous electrolyte present). The formation of epoxy groups on the carbon surface and their conversion to carbonates in the presence of $LiO_2$ was observed and provides direct evidence for carbon instability during battery discharge. Interestingly, studies by Thotiyl et al.[32] using acid treatment

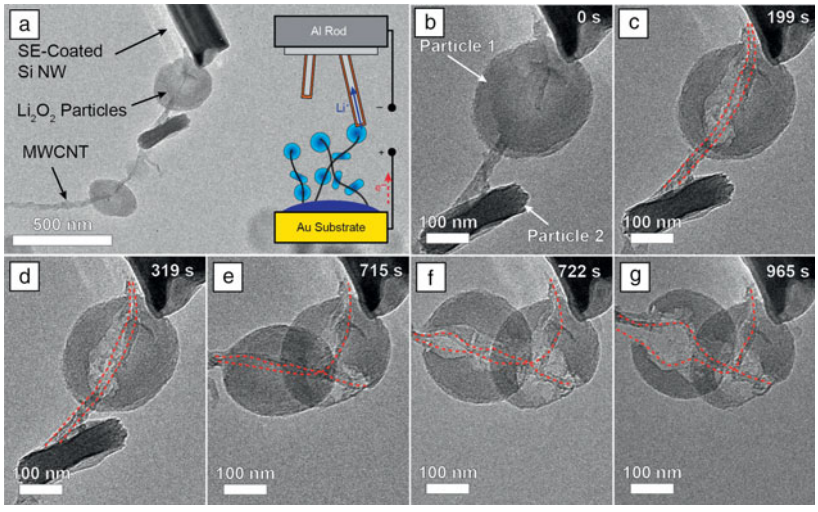


**Figure 3.** *In situ* transmission electron microscope (TEM) images showing oxidation of $Li_2O_2$ particles. (a) Schematic illustration of the *in situ* TEM microbattery superimposed over a low magnification TEM image of a solid electrolyte (SE)-coated Si nanowire contacting a single $Li_2O_2$ particle. (b) Higher magnification TEM image of the particles in (a) showing a multiwalled carbon nanotube (MWCNT) bundle contacting two physically separated $Li_2O_2$ particles labeled as Particle 1 and Particle 2, respectively. (c–g) Oxidation of Particles 1 and 2 during application of a 10 $V_{cell}$ potential to the MWCNT/$Li_2O_2$ positive electrode against the Si nanowire (NW) negative electrode. CNT axes are delineated by the red, dashed lines. Reprinted with permission from Reference 28. © 2013 American Chemical Society.

and Fenton's reagent, which quantify the amounts of side-reaction products formed from decomposition of the electrolyte and the carbon electrode respectively, revealed that on discharge, it is the decomposition of the electrolyte not the carbon electrode that dominates, forming $Li_2CO_3$ and carboxylate species. The degree of electrolyte decomposition depends on the type of carbon used. This finding was further confirmed in a recent study by McCloskey et al.[31] In addition to significant electrolyte decomposition during ORR, they also showed that the degree of parasitic reactions is sensitive to discharge rate (**Figure 4**b).[31] Further studies are required to elucidate the reaction mechanism responsible for electrolyte decomposition with and without carbon as a function of discharge rate, carbon chemistry, and electrolyte solvent and salt.

Turning to charging, DEMS experiments with isotopic carbon labeling show that carbon is unstable during $Li_2O_2$ oxidation above 3.5 V versus $Li/Li^+$: $CO_2$ is evolved, with the carbon originating from the carbon support in the oxygen electrode (**Figure 5**a–b).[29] The analysis of $^{13}C$ labeled cathodes at different states of charge with acid and Fenton's reagent has revealed that the process is complex. First, while the electrolyte continues to decompose, carbon electrode decomposition to form $Li_2CO_3$ becomes significant and grows to dominate at higher states of charge. The fact that carbon decomposition commences at 3.5 V, where $Li_2O_2$ starts to oxidize significantly, and not at 4 V, where carbon oxidation is expected, indicates that the process of carbon decomposition involves $Li_2O_2$ or its intermediates of oxidation. *In situ* DEMS shows that $Li_2CO_3$ simultaneously forms by decomposition of both the carbon cathode and the electrolyte and decomposes on charging. As a result, the amount of $O_2$ evolved on charge is not necessarily expected to be equal to that predicted by the amount of $Li_2O_2$ present at the end of discharge. An iodometric titration method has been developed to quantify the amount of $Li_2O_2$ present in the oxygen electrode and has confirmed this picture. When applied at different stages of discharge and charge[31] and combined with DEMS measurements of $O_2$ evolution and consumption, it has been shown the $Li_2O_2$ yield during charge is considerably less than 100%. This finding shows that not all $Li_2O_2$ present upon discharge evolves $O_2$ on charge (i.e., it partially participates in decomposition reactions), and confirms that carbon is relatively more unstable during charge than discharge.

*In situ* ambient pressure XPS measurements have shown highly reversible $Li_2O_2$ formation on a $Li_xV_2O_5$ surface in a solid-state cell,[33] thus highlighting the importance of the design of oxygen electrodes that are stable for Li-$O_2$ batteries to allow for long cycle life. In light of the observed instability of carbon, replacing it with a nanoporous gold electrode was found to provide stable cycling of Li-$O_2$ batteries.[7] As Au is heavy and expensive, TiC, TiN, Fe/N/C, N-doped carbon, and stainless steel have all been investigated as alternative materials to replace carbon.[34] Titration of each candidate cathode after each discharge/charge with acid and Fenton's reagent revealed the amount of inorganic carbonates such as $Li_2CO_3$ and organic carboxylate species, respectively, that were formed (Figure 5c–d). In comparison to carbon, TiC showed encouraging performance and stability, which is attributed to a layer of TiOC formed on its surface.[34]

## Searching for stable electrolytes

Early studies of Li-$O_2$ battery reactions employed carbonate-based electrolytes, where significant amounts of $Li_2CO_3$ and other organic side products were formed upon discharge.[35,36] Since then, a number of experimental[13] and computational[37] studies have shown that carbonates are highly susceptible to attack by the nucleophilic superoxide-related species (such as $O_2^-$ and $LiO_2$) formed during discharge. This highlights the importance of predisposition to superoxide attack as a key design criterion in selecting stable electrolyte solvents.[13,25,35,38–40]

Unlike carbonates, there are several classes of electrolytes that support formation of $Li_2O_2$ as the majority species during battery discharge (Figure 4a),[7,25,41–51] albeit with varying degrees of side reactivity, as discussed later. This emphasizes the difficulty in finding electrolytes stable toward the strong nucleophiles $O_2^-/LiO_2$ that are intermediates in $Li_2O_2$ formation, as well as toward $Li_2O_2$ itself.[37] In the search for stable electrolytes, several experimental and theoretical approaches are being pursued: (1) Modeling of the reactions between $O_2^-/LiO_2$ and the solvent (e.g., by density functional theory),[37] (2) chemical screening using $KO_2$,[21,52] (3) electrochemical measurements

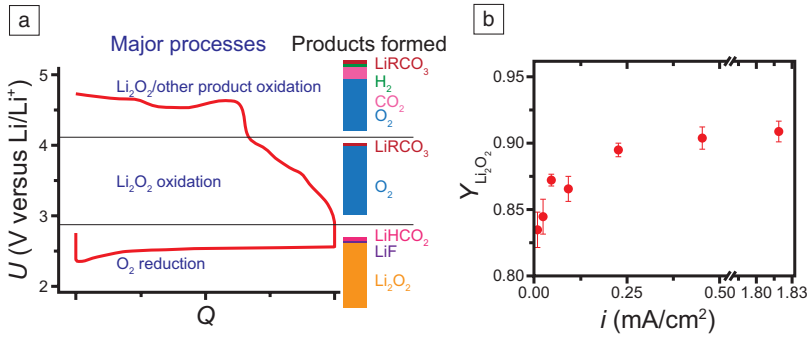


**Figure 4.** (a) Discharge-charge curve showing evolution of reaction potential ($U$) with charge passed ($Q$) of a carbon paper-based cathode in 1 M LiTFSI ($Li(CF_3SO_2)_2N$) in dimethoxyethane, along with reaction product quantification during oxygen reduction reaction and oxygen evolution reaction using iodometric titration and nuclear magnetic resonance techniques. Reaction product quantification shows that $Li_2O_2$ is the dominant product on discharge (along with carbonate species, R = Li or $CH_3$), while $CO_2$ and $H_2O$ are evolved during charge as a result of electrolyte decomposition. (b) Yield of $Li_2O_2$ ($Y_{Li_2O_2}$) as a function of Li-$O_2$ battery discharge rate ($i$) for the same cathode, showing greater chemical reactivity between $Li_2O_2$ and the electrolyte at lower rates. Reprinted with permission from Reference 31. © 2013 American Chemical Society.

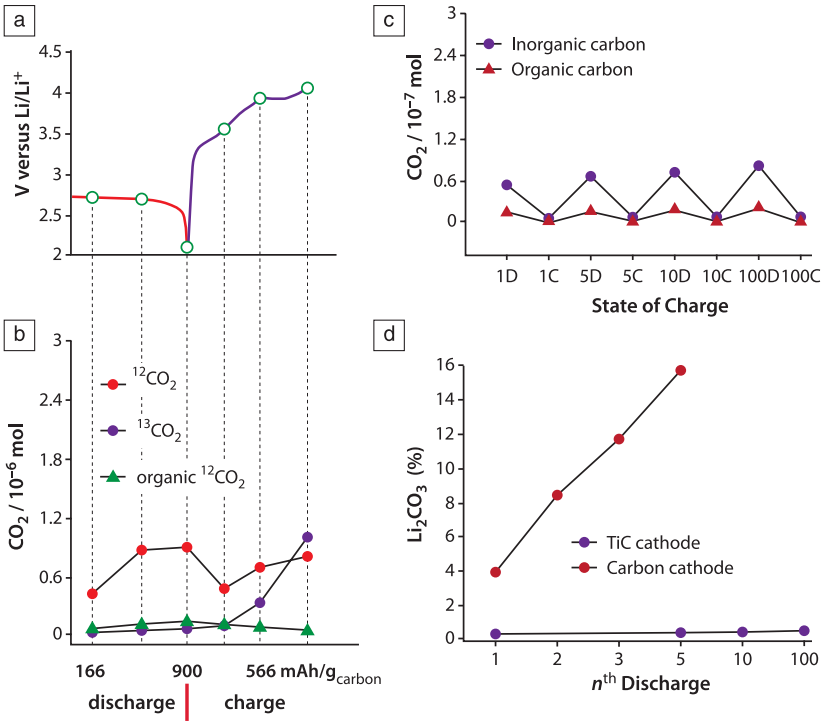


**Figure 5.** Quantification of carbon-containing by-products in carbon and TiC cathodes on discharge and charge, respectively. Data demonstrate significant side reactions both on discharge and charge at carbon electrodes. These are greatly suppressed at TiC cathodes. (a) Discharge-charge curve of a carbon cathode in 0.1 M $LiClO_4$/dimethyl sulfoxide electrolyte on the first cycle. (b) Moles of $CO_2$ evolved from the cathode stopped at certain points of discharge/charge indicated in (a) and then treated to decompose $Li_2CO_3$ and lithium carboxylates.[32] (c) The same procedure applied to TiC electrodes in the same electrolyte at the indicated numbers of discharge (1D, 5D, . . . ) and charge (1C, 5C, . . . ); shown are inorganic and organic carbonaceous products. (d) Evolution of percentage of carbonate products with cycle number at a carbon and TiC electrode, respectively.[34] Reprinted with permission from Reference 32. © 2013 American Chemical Society and Reference 34. © 2013 Nature Publishing Group.

(e.g., cyclic voltammetry or rotating electrodes),[41,53–56] and (4) analysis of the reactions occurring at the cathode in a Li-$O_2$ cell using a combination of spectroscopic methods (e.g., Fourier transform infrared [FTIR], powder x-ray diffraction, nuclear magnetic resonance, SERS, XPS, mass spectrometry, and $Li_2O_2$ titration).[7,42–44,57–59]

## Ether electrolytes

Recent extensive investigation of nonaqueous electrolytes for Li-$O_2$ cells, based on ethers, amides, ionic liquids (ILs), and DMSO, have shown that they all predominantly support the formation of $Li_2O_2$ upon first discharge and its removal on recharge.[32,44–46] Ethers are attractive for the Li–$O_2$ battery because they are safe, cheap, compatible with lithium metal anodes, more stable toward reduced $O_2$ species compared with organic carbonates, and have relatively high oxidation windows (up to 4 V versus $Li/Li^+$), and low volatilities (for longer-chain ethers). However, there is growing experimental and theoretical evidence that ether-based electrolytes are not suitable for Li-$O_2$ cells.[13,29,31,44,60–62] Ethers are known to form peroxides under ambient conditions by auto oxidation reactions.[63] This instability toward auto oxidation has been identified as a possible pathway of initial attack of the solvent that gives rise to further decomposition reactions **Figure 6**b).[61]

## Amide electrolytes

Amides are a major class of solvent that are known to be highly stable against bases and nucleophilic attack and have been extensively used for $O_2$ reduction studies.[64,65] Theoretical calculations and $KO_2$ screening studies suggest high-energy barriers against nucleophilic substitution at the carbons due to unfavorable stability of the reaction products.[61] Calculations also show that amides are much more stable against auto oxidation than ethers; amides require a high activation energy for proton abstraction by $O_2^-$.[37] Dimethylformamide (DMF) and dimethylacetamide (DMA) have been investigated as the basis of electrolytes for Li-$O_2$ batteries.[42,47] DMF shows greater stability than ethers, but some parasitic reactions occur, and significant capacity fading is observed.[47] Cells with DMA electrolyte demonstrate better performance, up to 80 cycles with a reproducible voltage profile.[42]

## Ionic liquids and DMSO

Chemical screening by $KO_2$ and voltammetric methods suggest that the stability of IL electrolytes is much greater than organic carbonate solvents.[41,48–51] However, due to the difficulty of purifying ILs, the impurities that remain may be the reason for the observed parasitic reactions that compromised cycleability.

Cells based on DMSO, which have been used to study $O_2$ reduction in nonaqueous media in the past,[66] have shown sustained cycling, with the reversible formation/decomposition of $Li_2O_2$ at the cathode.[7,34] FTIR analysis of the discharge product in a carbon cathode in 1M $LiClO_4$ in DMSO confirms dominant formation of $Li_2O_2$, along with some $Li_2CO_3$ and HCOOLi.[7,31,34,62]

Further research on the stability of nonaqueous electrolytes and electrode materials in rechargeable Li-$O_2$ batteries is much needed. Reactions do not proceed without side reactions; therefore, the question is not whether side reactions occur but what degree of stability is required. In this respect, two effects need to be considered: First, the extent of the side reactions, decomposition of solvent, salt, electrode, or binder to form solid, gaseous, or dissolved side products, which deplete the particular component and will lead to failure once a threshold of consumption is exceeded; and second, the nature of the side reaction products and their effects on the reversible electrochemistry. In this regard, the products of the

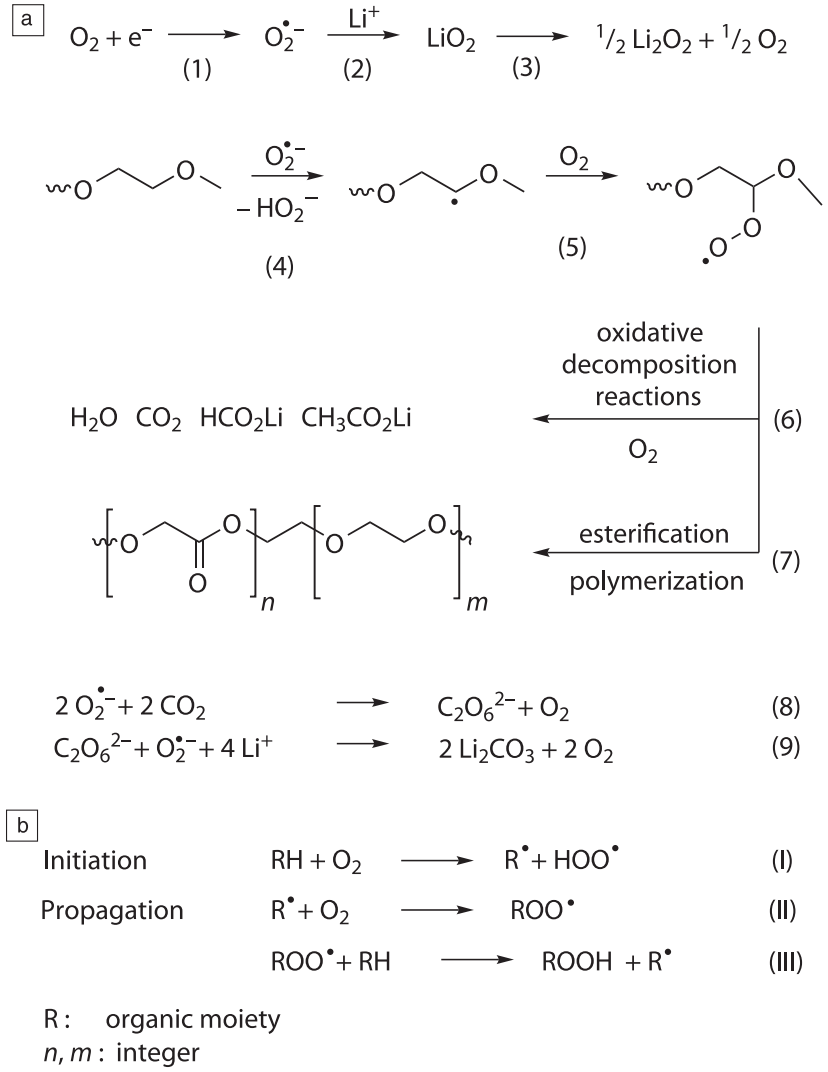


**Figure 6.** Possible reaction schemes for ether decomposition. (a) Proposed reaction scheme on discharge to explain decomposition of ether: electron reduction of $O_2$ to superoxide (1), binding with $Li^+$ (2), and disproportionation to $Li_2O_2$ (3) as the ideal sequence. Alternatively, superoxide may abstract a proton from the solvent (4) to give hydroperoxide (5), which may further react in a series of oxidative decomposition steps (6) or yield esters or polymeric compounds (7). Superoxide and $CO_2$ from step (6) react to form $Li_2CO_3$ (8 and 9). (b) Alternative possible pathway with initial attack by autoxidation to give hydroperoxyl and alkyl radicals (I) and chain propagation by $O_2$ addition and further proton abstraction (II and III). Note: The dot (•) denotes a free radical. (a) Reprinted with permission from Reference 44. © 2012 American Chemical Society. (b) Reprinted with permission from Reference 61. © 2011 American Chemical Society.

parasitic reactions should not passivate the electrode significantly (e.g., the by-products should diffuse away from the surface). If they cannot, they have to be able to decompose easily on charge without introducing a significant overpotential; otherwise, a relatively small degree of decomposition can have a disproportionately large detrimental effect on the electrochemistry. This is what happens with carbon electrodes and many electrolytes, which form solid insulating $Li_2CO_3$ on the electrode surface, leading to severe polarization and premature cell death. It may be that the combination of DMSO with a nanoporous Au cathode produces side products other than $Li_2CO_3$, thus avoiding large polarization.

## Challenges and opportunities: Aqueous lithium-oxygen batteries

In the second part of this article, we will discuss recent efforts in protected lithium metal as the negative electrode in aqueous Li-$O_2$ batteries. Aqueous batteries have received significantly less attention than nonaqueous Li-$O_2$ batteries due to the practical challenges involved with preventing a violent reaction between lithium and water. Developing lithium metal as the negative electrode that can cycle safely and stably has been a challenge for 40 years, owing to the dendrites that form on repeated lithium dissolution and lithium deposition. Dendrites can be fatal to battery performance since they pose the risk of growing into the cathode and causing a short circuit and battery failure. There are still no rechargeable lithium anode-based batteries on the market; all rechargeable Li-ion batteries have thus far contained the lithium inside another material such as aluminum (LiAl),[67,68] carbon ($LiC_6$),[15,16,69] and, more recently, tin[15,70,71] and silicon.[72]

Zhang et al.[70] have reported lithium dendrite formation in a typical nonaqueous electrolyte containing polyethylene glycol dimethyl ether (PEGDME, Mw. 250) with $Li(CF_3SO_2)_2N$ (LiTFSI) for lithium-air rechargeable Li-$O_2$ batteries. The Li/PEGDME-LiTFSI/Li cell showed short circuits after 21.4 h of polarization at 0.2 mA $cm^{-2}$ and 4.0 h of polarization at 1.0 mA $cm^{-2}$. A lithium metal alloy with aluminum solved the dendrite issue,[71] but alloy electrodes survive only a limited number of cycles owing to extreme changes in volume during operation.

To reduce lithium dendrite formation, solid electrolytes have been developed for electric vehicle applications.[72] Theoretical calculations suggest that a homogenous solid-state electrolyte with a modulus of 6 GPa would drastically reduce dendrite formation.[73] As the moduli of ceramic materials are generally higher than 6 GPa, little or no lithium dendrite formation between a ceramic lithium-ion conductor and lithium metal is expected. Visco et al.[69] and Stevens et al.[74] first reported experimental evidence of the feasibility of protected lithium metal electrodes, with Li/$Li_3N$/$Li_{1+x}Al_xTi_{2-x}(PO_4)_3$ (LATP) and Li/$Li_{3-x}PO_{4-y}N_y$/LATP, respectively. $Li_3N$ and $Li_{3-x}PO_{4-y}N_y$ are used to prevent direct contact of lithium metal with LATP, since LATP is electrochemically unstable at the potential of metallic lithium.[11,12,75] Aqueous Li-$O_2$ batteries assembled with these lithium electrodes could be cycled

at 1 mA $cm^{-2}$ and room temperature without degradation of the cell performance for a short period of 10 min.[69,73] Subsequently, other protected lithium anodes based on garnet-type solid electrolytes[76] and polymer-ceramic composite membranes[77] have been reported.

While ceramic conductors are stiff enough to prevent lithium dendrite growth, they do not easily make low-resistance contacts with other solid components and thus have high charge transfer resistance. Recent research efforts have been focused on using polymer-ceramic composite electrolytes to form a conformal interface and reduce interfacial resistance. Rosso et al. investigated the mechanism of lithium dendrite growth in Li/PEO-based-electrolyte/Li (PEO = polyethylene oxide),[78,79] where the onset of dendrite formation and the time to reach short-circuit times can be studied by direct *in situ* observation and simultaneous cell voltage monitoring. **Table I** summarizes the dendrite onset and short-circuit time for different compositions of PEO-based electrolytes. No dendrite formation was observed in a Li/$PEO_{20}$LiTFSI/Li cell at a low current density of 0.03 mA $cm^{-2}$ for 100 h at 80°C, while at a high current density of 0.7 mA $cm^{-2}$, dendrites were observed after less than 1 h of deposition.[79] Such lithium dendrite formation onset times at high current density are too short to be used in practical applications. The use of ceramic or IL additives in polymer electrolytes comprises another strategy to suppress dendrite formation. The addition of nano-$SiO_2$ and/or IL of *N*-methyl-*N*-propylpiperidinium TFSI (PP13TFSI)[80,81] to polymer electrolytes has been shown to increase the onset time of dendrite formation from 10 h for Li/$PEO_{18}$TFSI/Li to 21 h at 1.0 mA $cm^{-2}$ at 60°C. **Figure 7**a shows the cycling performance of the lithium deposition and dissolution process in a Li/$PEO_{18}$LiTFSI-$SiO_2$-PP13TFSI/Li cell at 60°C, where the cell voltage showed no significant change during cycling, and no dendrite formation was detected at a current density of 0.3 mA $cm^{-2}$ for 30 h.[81]

Based on these positive results, this composite polymer electrolyte of $PEO_{18}$LiTFSI-$SiO_2$-PP13TFSI was also assessed as the protected lithium-metal anode for rechargeable lithium-air batteries. Figure 7b shows reversible cycling of a Li/$PEO_{18}$LiTFSI-PP13TFSI/LATP/aqueous 1 M LiCl-0.004 M LiOH/Pt, air cell at 0.3 mA $cm^{-2}$ and 60°C,[82] with LATP as the solid electrolyte. The inclusion of PP13TFSI IL is effective in reducing interfacial resistance between lithium and the electrolyte and facilitating highly reversible Li-$O_2$ cycling.

While the early onset of lithium dendrite formation and low output power remain yet to be completely solved, recent research has shown that these challenges are closely related to the physical properties of the solid electrolyte used. Further materials development for the protection layer of lithium is therefore essential to achieve high power density at several mA $cm^{-2}$ and extended deep cycling of the lithium electrode for Li-$O_2$ batteries.

**Table I. Dependence of lithium dendrite formation onset time ($t_o$) and short-circuit time ($t_s$) on electrolyte formulation, temperature, and current density.**

| Electrolyte | Temperature (°C) | Current density ($mAcm^{-2}$) | Onset time (hour) | Short circuit time (hour) | Ref. |
|---|---|---|---|---|---|
| PEGDME-LiTFSI (Li/O = 1/20) | room temperature | 0.2 | | 21 | 70 |
| | | 1.0 | | 4 | |
| PEGDME-LiTFSI (Li/O = 1/20)- 20 wt% $SiO_2$ | room temperature | 0.2 | | 110 | 70 |
| | | 1.0 | | 20 | |
| PVdF-HFP-$SiO_2$-EC-PC-LiTFSI | room temperature | 0.6 | | 14 | 83 |
| | | | | | |
| PEO-LiTFSI (Li/O = 1/20) | 80 | 0.05 | 38 | 110 | 78 |
| $PEO_{18}$LiTFSI-1.44PP13TFSI | 60 | 0.1 | 125 | 235 | 80 |
| | | 1.0 | 10 | 15 | |
| $PEO_{18}$LiTFSI-1.44PP13TFSI-10 wt% $SiO_2$ | 60 | 0.1 | 460 | 672 | 84 |
| | | 1.0 | 21 | 37 | |

Note: PVdF, polyvinylidene fluoride; HFP, hexafluorophosphate; EC, ethylene carbonate; PC, propylene carbonate; PEO, polyethylene oxide; LiTFSI, $Li(CF_3SO_2)_2N$; PEGDME, polyethylene glycol dimethyl ether; PP13, *N*-methyl-*N*-propylpiperidinium.

## Summary

The need for storage technologies with much greater gravimetric energy than Li-ion batteries makes Li-$O_2$ batteries an attractive energy storage option for applications that require high-energy density such as electric vehicles. Although notable progress has been made in the development of rechargeable, lab-scale nonaqueous Li-$O_2$ cells, further investigation of the oxygen reduction reaction (ORR) and oxygen evolution reaction (OER) in nonaqueous electrolytes, and parasitic reaction mechanisms involving inactive components in the oxygen electrode is required in order to aid the rational design and development of kinetically facile and chemically stable electrode and electrolyte configurations.

As detailed in this review, researchers have just begun to connect the physical properties (morphology and surface versus bulk chemistry) of $Li_2O_2$ with the corresponding kinetics of $Li_2O_2$ formation and oxidation. Important topics warranting further investigation in this area include the detailed reaction and growth mechanisms of $Li_2O_2$ at high and low overpotentials; the electronic nature (surface and bulk) of electrochemically formed $Li_2O_2$; intrinsic $Li_2O_2$ oxidation pathways; and the influence of non-carbonate solvents on the nucleation and growth of $Li_2O_2$ and its oxidation.

As carbon is not stable in the oxygen electrode, improved morphological, chemical, and kinetic understanding of Li-$O_2$ reactions in non-carbon electrodes will become increasingly relevant for

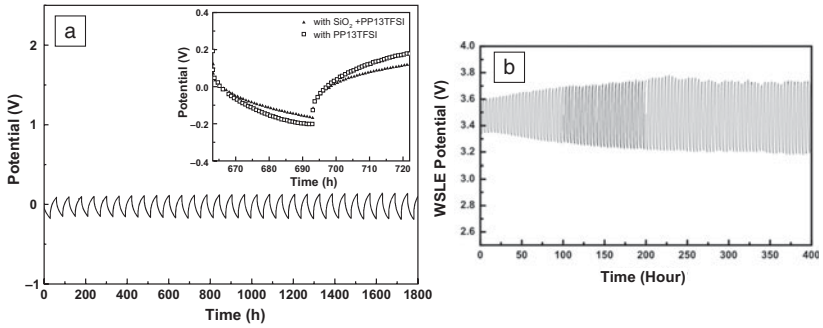


**Figure 7.** (a) Cycling performance for the Li/$PEO_{18}$LiTFSI-$SiO_2$-PP13TFSI/Li cell at 0.3 mA $cm^{-2}$ and 60°C. The inset shows a comparison of the 11th cycle for Li/$PEO_{18}$LiTFSI-$SiO_2$-PP13TFSI/Li and Li/$PEO_{18}$LiTFSI-PP13TFSI/Li. Cycling performance of the Li/$PEO_{18}$LiTFSI-1.44PP13TFSI/LATP/aqueous 1 M LiCl-0.004 M LiOH/Pt-air cell at 0.3 mA $cm^{-2}$ and 60°C between (b) 0 h and 400 h. The water-stable lithium electrode (WSLE) voltage was measured by a Pt-air reference electrode. Discharge and charge period are both two hours. Cycle was repeated without interval. Microscopic observations of the cell indicated no dendrite formation after cycling. Note: PEO, polyethylene oxide; LiTFSI, $Li(CF_3SO_2)_2N$; PP13, *N*-methyl-*N*-propylpiperidinium; LATP, $Li_{1+x}Al_xTi_{2-x}(PO_4)_3$. (a) Reprinted with permission from Reference 81. © 2014 Elsevier. (b) Reprinted with permission from Reference 82. © 2014 The Electrochemical Society.

the development of rechargeable Li-$O_2$ batteries. The search for electrolytes that are chemically stable against the oxygen electrode is another major focus of research. The discovery that reduced oxygen species produced during ORR are also highly reactive against a broad range of electrolyte solvents has spurred detailed spectroscopic, spectrometric, and titration studies examining the interplay between electrolyte formulation and discharge reaction product. Combining these experimental approaches with theoretical calculations evaluating electrolyte susceptibility to attack by $Li_2O_2$ and/or ORR intermediates will be crucial to finding an electrolyte that is moderately stable during ORR, but also possesses a favorable synergy with the chosen electrode material such that parasitic reactions during OER are minimized.

Significant progress has been made toward finding materials that suppress lithium dendrite formation and also adequately protect the lithium metal anode from contact with reactive gases and water in both nonaqueous and aqueous Li-$O_2$ battery environments. Representing a compromise between the favorable transport properties of liquid and the high mechanical stability of solid electrolytes, the use of polymers has emerged as a particularly promising strategy to protect lithium metal anodes. Further research into the possibility of incorporating nanostructured additives to improve power capabilities while maintaining chemical stability against lithium metal in full Li-$O_2$ cells is a promising direction for future efforts in this field. The need for fundamentally understanding the relationship between electrode reaction mechanisms and parasitic processes occurring in rechargeable Li-$O_2$ batteries presents an opportunity to combine cutting edge experimental and computational techniques with materials innovation in the areas outlined previously to enable the development of practical rechargeable Li-$O_2$ batteries, which combine high rate capability with high round-trip efficiency and long cycle life.

## Acknowledgments

Y.S-H., N.O.-V. and D.G.K. gratefully acknowledge the Robert Bosch Company for a Bosch Energy Research Network Grant, the CERC-CVC US China Clean Energy Research Center-Clean Vehicles Consortium of the Department of Energy (under award number DE—PI0000012), and the MRSEC program of the National Science Foundation for their generous support (under award number DMR—0819762). N.O.-V. acknowledges a Marie Curie International Outgoing Fellowship within the seventh European Community Framework Programme (2012). P.G.B. acknowledges the EPSRC for financial support, including the SUPERGEN program. S.A.F. acknowledges financial support by the Austrian Federal Ministry of Economy, Family and Youth and the Austrian National Foundation for Research, Technology and Development.

## References

1. Y.-C. Lu, B.M. Gallant, D.G. Kwabi, J.R. Harding, R.R. Mitchell, M.S. Whittingham, Y. Shao-Horn, *Energy Environ. Sci.* **6**, 750 (2013).
2. J.-S. Lee, S. Tai Kim, R. Cao, N.-S. Choi, M. Liu, K.T. Lee, J. Cho, *Adv. Energy Mater.* **1**, 34 (2011).
3. P.G. Bruce, S.A. Freunberger, L.J. Hardwick, J.-M. Tarascon, *Nat. Mater.* **11**, 19 (2012).
4. J. Christensen, P. Albertus, R.S. Sanchez-Carrera, T. Lohmann, B. Kozinsky, R. Liedtke, J. Ahmed, A. Kojic, *J. Electrochem. Soc.* **159**, R1 (2012).
5. P.G. Bruce, L.J. Hardwick, K.M. Abraham, *MRS Bull.* **36**, 506 (2011).
6. Y. Shao, S. Park, J. Xiao, J.-G. Zhang, Y. Wang, J. Liu, *ACS Catal.* **2**, 844 (2012).
7. Z. Peng, S.A. Freunberger, Y. Chen, P.G. Bruce, *Science* **337**, 563 (2012).
8. B.M. Gallant, R.R. Mitchell, D.G. Kwabi, J. Zhou, L. Zuin, C.V. Thompson, Y. Shao-Horn, *J. Phys. Chem. C* **116**, 20800 (2012).
9. S.H. Oh, L.F. Nazar, *Adv. Energy Mater.* **2**, 903 (2012).
10. Z.-L. Wang, D. Xu, J.-J. Xu, L.-L. Zhang, X.-B. Zhang, *Adv. Funct. Mater.* **22**, 3699 (2012).
11. S. Hasegawa, N. Imanishi, T. Zhang, J. Xie, A. Hirano, Y. Takeda, O. Yamamoto, *J. Power Sources* **189**, 371 (2009).
12. N. Imanishi, S. Hasegawa, T. Zhang, A. Hirano, Y. Takeda, O. Yamamoto, *J. Power Sources* **185**, 1392 (2008).
13. B.D. McCloskey, D.S. Bethune, R.M. Shelby, G. Girishkumar, A.C. Luntz, *J. Phys. Chem. Lett.* **2**, 1161 (2011).
14. H. Ikeda, R. Hoch, R. Hausslein, US Patent 05879836 (1999).
15. H. Xia, L. Lu, G. Ceder, *J. Power Sources* **159**, 1422 (2006).
16. Y. Zhu, C. Wang, *J. Phys. Chem. C* **114**, 2830 (2010).
17. K. Kang, Y.S. Meng, J. Bréger, C.P. Grey, G. Ceder, *Science* **311**, 977 (2006).
18. H. Chen, M. Armand, G. Demailly, F. Dolhem, P. Poizot, J.-M. Tarascon, *ChemSusChem* **1**, 348 (2008).
19. B.M. Gallant, D.G. Kwabi, R.R. Mitchell, J. Zhou, C.V. Thompson, Y. Shao-Horn, *Energy Environ. Sci.* **6**, 2518 (2013).
20. R.R. Mitchell, B.M. Gallant, C.V. Thompson, Y. Shao-Horn, *Energy Environ. Sci.* **4**, 2952 (2011).
21. R. Black, S.H. Oh, J. Lee, T. Yim, B. Adams, L.F. Nazar, *J. Am. Chem. Soc.* **134**, 2902 (2012).
22. D. Xu, Z. Wang, J. Xu, L. Zhang, X. Zhang, *Chem. Commun.* **48**, 6948 (2012).
23. R.R. Mitchell, B.M. Gallant, Y. Shao-Horn, C.V. Thompson, *J. Phys. Chem. Lett.* **4**, 1060 (2013).
24. J.S. Hummelshøj, A.C. Luntz, J.K. Nørskov, *J. Chem. Phys.* **138**, 034703 (2013).
25. Z. Peng, S.A. Freunberger, L.J. Hardwick, Y. Chen, V. Giordani, F. Bardé, P. Novák, D. Graham, J.-M. Tarascon, P.G. Bruce, *Angew. Chem. Int. Ed. Engl.* **50**, 6351 (2011).

26. B.D. Adams, C. Radtke, R. Black, M.L. Trudeau, K. Zaghib, L.F. Nazar, *Energy Environ. Sci.* **6**, 1772 (2013).
27. D. Zhai, H.-H. Wang, J. Yang, K.C. Lau, K. Li, K. Amine, L.A. Curtiss, *J. Am. Chem. Soc.* **135**, 15364 (2013).
28. L. Zhong, R.R. Mitchell, Y. Liu, B.M. Gallant, C.V. Thompson, J.Y. Huang, S.X. Mao, Y. Shao-Horn, *Nano Lett.* **13**, 2209 (2013).
29. B.D. McCloskey, A. Speidel, R. Scheffler, D.C. Miller, V. Viswanathan, J.S. Hummelshøj, J.K. Nørskov, A.C. Luntz, *J. Phys. Chem. Lett.* **3**, 997 (2012).
30. D.M. Itkis, D.A. Semenenko, E.Y. Kataev, A.I. Belova, V.S. Neudachina, A.P. Sirotina, M. Hävecker, D. Teschner, A. Knop-Gericke, P. Dudin, A. Barinov, E.A. Goodilin, Y. Shao-Horn, L.V. Yashina, *Nano Lett.* **13**, 4697 (2013).
31. B.D. McCloskey, A. Valery, A.C. Luntz, S.R. Gowda, G.M. Wallraff, J.M. Garcia, T. Mori, L.E. Krupp, *J. Phys. Chem. Lett.* **4**, 2989 (2013).
32. M.M. Ottakam Thotiyl, S.A. Freunberger, Z. Peng, P.G. Bruce, *J. Am. Chem. Soc.* **135**, 494 (2012).
33. Y.-C. Lu, E.J. Crumlin, G.M. Veith, J.R. Harding, E. Mutoro, L. Baggetto, N.J. Dudney, Z. Liu, Y. Shao-Horn, *Sci. Rep.* **2**, 715 (2012).
34. M.M. Ottakam Thotiyl, S.A. Freunberger, Z. Peng, Y. Chen, Z. Liu, P.G. Bruce, *Nat. Mater.* **12**, 1050 (2013).
35. F. Mizuno, S. Nakanishi, Y. Kotani, S. Yokoishi, H. Iba, *Electrochemistry* **78**, 403 (2010).
36. W. Xu, V.V. Viswanathan, D. Wang, S.A. Towne, J. Xiao, Z. Nie, D. Hu, J.-G. Zhang, *J. Power Sources* **196**, 3894 (2011).
37. V.S. Bryantsev, J. Uddin, V. Giordani, W. Walker, D. Addison, G.V. Chase, *J. Electrochem. Soc.* **160**, A160 (2012).
38. D.T. Sawyer, J.L. Roberts, Jr., *J. Electroanal. Chem.* **12**, 90 (1966).
39. C.O. Laoire, S. Mukerjee, K.M. Abraham, E.J. Plichta, M.A. Hendrickson, *J. Phys. Chem. C* **113**, 20127 (2009).
40. R. Younesi, M. Hahlin, F. Björefors, P. Johansson, K. Edström, *Chem. Mater.* **25**, 77 (2012).
41. J. Herranz, A. Garsuch, H.A. Gasteiger, *J. Phys. Chem. C* **116**, 19084 (2012).
42. W. Walker, V. Giordani, J. Uddin, V.S. Bryantsev, G.V. Chase, D. Addison, *J. Am. Chem. Soc.* **135**, 2076 (2013).
43. F. Mizuno, K. Takechi, S. Higashi, T. Shiga, T. Shiotsuki, N. Takazawa, Y. Sakurabayashi, S. Okazaki, I. Nitta, T. Kodama, H. Nakamoto, H. Nishikoori, S. Nakanishi, Y. Kotani, H. Iba, *J. Power Sources* **228**, 47 (2013).
44. S.A. Freunberger, Y. Chen, N.E. Drewett, L.J. Hardwick, F. Bardé, P.G. Bruce, *Angew. Chem. Int. Ed. Engl.* **50**, 8609 (2011).
45. C. Laoire, S. Mukerjee, E.J. Plichta, M.A. Hendrickson, K.M. Abraham, *J. Electrochem. Soc.* **158**, A302 (2011).
46. M. Leskes, N.E. Drewett, L.J. Hardwick, P.G. Bruce, G.R. Goward, C.P. Grey, *Angew. Chem. Int. Ed. Engl.* **51**, 8560 (2012).
47. Y. Chen, S.A. Freunberger, Z. Peng, F. Bardé, P.G. Bruce, *J. Am. Chem. Soc.* **134**, 7952 (2012).
48. F. Mizuno, S. Nakanishi, A. Shirasawa, K. Takechi, T. Shiga, H. Nishikoori, H. Iba, *Electrochemistry* **79**, 876 (2011).
49. K. Takechi, S. Higashi, F. Mizuno, H. Nishikoori, H. Iba, T. Shiga, *ECS Electrochem. Lett.* **1**, A27 (2012).
50. S. Monaco, A.M. Arangio, F. Soavi, M. Mastragostino, E. Paillard, S. Passerini, *Electrochim. Acta* **83**, 94 (2012).
51. C.J. Allen, J. Hwang, R.A. Kautz, S. Mukerjee, E.J. Plichta, M.A. Hendrickson, K.M. Abraham, *J. Phys. Chem. C* **116**, 20755 (2012).
52. K.U. Schwenke, S. Meini, X. Wu, H.A. Gasteiger, M. Piana, *Phys. Chem. Chem. Phys.* **15**, 11830 (2013).
53. D. Aurbach, M. Daroux, P. Faguy, E. Yeager, *J. Electroanal. Chem. Interfacial Electrochem.* **297**, 225 (1991).
54. V.S. Bryantsev, V. Giordani, W. Walker, M. Blanco, S. Zecevic, K. Sasaki, J. Uddin, D. Addison, G.V. Chase, *J. Phys. Chem. A* **115**, 12399 (2011).
55. C.O. Laoire, S. Mukerjee, K.M. Abraham, E.J. Plichta, M.A. Hendrickson, *J. Phys. Chem. C* **114**, 9178 (2010).
56. C.J. Allen, S. Mukerjee, E.J. Plichta, M.A. Hendrickson, K.M. Abraham, *J. Phys. Chem. Lett.* **2**, 2420 (2011).
57. H.-G. Jung, J. Hassoun, J.-B. Park, Y.-K. Sun, B. Scrosati, *Nat. Chem.* **4**, 579 (2012).
58. Y.-C. Lu, H.A. Gasteiger, Y. Shao-Horn, *J. Am. Chem. Soc.* **133** (47), 19048 (2011).
59. S.H. Oh, R. Black, E. Pomerantseva, J.-H. Lee, L.F. Nazar, *Nat. Chem.* **4**, 1004 (2012).
60. R. Younesi, M. Hahlin, M. Treskow, J. Scheers, P. Johansson, K. Edstrom, *J. Phys. Chem. C* **116**, 18597 (2012).
61. V.S. Bryantsev, F. Faglioni, *J. Phys. Chem. A* **116**, 7128 (2012).
62. K.R. Ryan, L. Trahey, B.J. Ingram, A.K. Burrell, *J. Phys. Chem. C* **116**, 19724 (2012).
63. A.M. Clover, *J. Am. Chem. Soc.* **44**, 1107 (1922).
64. D.T. Sawyer, J.S. Valentine, *Acc. Chem. Res.* **14**, 393 (1981).
65. M.E. Peover, B.S. White, *Electrochim. Acta* **11**, 1061 (1966).
66. M.V Merritt, D.T. Sawyer, *J. Org. Chem.* **35**, 2157 (1970).
67. Y.-I. Jang, B.J. Neudecker, N.J. Dudney, *Electrochem. Solid-State Lett.* **4**, A74 (2001).
68. M.D. Levi, D. Aurbach, *J. Phys. Chem. B* **101**, 4630 (1997).
69. S. Visco, B. Katz, M.Y. Chu, L. De Jonghe, Eds., *Symposium on Scalable Energy Storage: Beyond Lithium-Ion* (IBM, Almaden Institute, San Jose, CA 2009).
70. X.-W. Zhang, Y. Li, S.A. Khan, P.S. Fedkiw, *J. Electrochem. Soc.* **151**, A1257 (2004).
71. B.M.L. Rao, R.W. Francis, H.A. Christopher, *J. Electrochem. Soc.* **124**, 1490 (1977).
72. S. Megahed, B. Scrosati, *Electrochem. Soc. Interface* **4**, 34 (1995).
73. C. Monroe, J. Newman, *J. Electrochem. Soc.* **152**, A396 (2005).
74. P. Stevens, G. Toussaint, G. Caillon, P. Viaud, P. Vinatier, C. Cantau, O. Fichet, C. Sarrazin, M. Mallouki, *ECS Trans.* **28**, 1 (2010).
75. D. Capsoni, M. Bini, S. Ferrari, E. Quartarone, P. Mustarelli, *J. Power Sources* **220**, 253 (2012).
76. R. Murugan, V. Thangadurai, W. Weppner, *Angew. Chem. Int. Ed. Engl.* **46**, 7778 (2007).
77. B. Kumar, J. Kumar, R. Leese, J.P. Fellner, S.J. Rodrigues, K.M. Abraham, *J. Electrochem. Soc.* **157**, A50 (2010).
78. M. Rosso, T. Gobron, C. Brissot, J.-N. Chazalviel, S. Lascaud, *J. Power Sources* **97–98**, 804 (2001).
79. C. Brissot, M. Rosso, J.-N. Chazalviel, S. Lascaud, *J. Power Sources* **81–82**, 925 (1999).
80. S. Liu, N. Imanishi, T. Zhang, A. Hirano, Y. Takeda, O. Yamamoto, J. Yang, *J. Electrochem. Soc.* **157**, A1092 (2010).
81. S. Liu, H. Wang, N. Imanishi, T. Zhang, A. Hirano, Y. Takeda, O. Yamamoto, J. Yang, *J. Power Sources* **196**, 7681 (2011).
82. T. Zhang, N. Imanishi, A. Hirano, Y. Takeda, O. Yamamoto, *Electrochem. Solid-State Lett.* **14**, A45 (2011).
83 L. Sannier, R. Bouchet, M. Rosso, J.-M. Tarascon, *J. Power Sources* **158**, 564 (2006).
84. W. Xu, K. Xu, V.V. Viswanathan, S.A. Towne, J.S. Hardy, J. Xiao, Z. Nie, D. Hu, D. Wang, J.-G. Zhang, *J. Power Sources* **196**, 9631 (2011). □